Experimental and Numerical Investigation on Coupled Motion Characteristics of a Tunnel Element Suspended from a Twin-barge

Can Yang [a], Sam D. Weller [b], Yong-xue Wang [a], De-zhi Ning [a], Lars Johanning [b,a,*]

[a] State Key Laboratory of Coastal and Offshore Engineering, Dalian University of Technology (DUT), Dalian 116024, China

[b] College of Engineering, Mathematics and Physical Sciences, University of Exeter, Penryn Campus, Penryn, Cornwall, TR10 9FE, UK

Abstract: The coupled motion characteristics of a tunnel element, which is suspended from a twin-barge and moored to the seabed during the installation process, has been investigated using a 1:50 scaled model. Response characteristics are obtained for multiple regular wave conditions and three different immersion depths. Experimental investigation includes studies to identify system properties of individual arrangements (tunnel, twin-barge) and for the coupled tunnel & twin-barge configuration. Investigation of motion characteristics includes i) experimental studies of the tunnel element from a fixed suspension point and barge, ii) experimental studies with and without a mooring arrangement from the tunnel element to the seabed, iii) experimental study of the fully coupled tunnel & twin-barge configuration, and iv) numerical investigation of the fully coupled tunnel & twin-barge configuration using a commercial fully dynamic mooring simulation software (OrcaFlex^{TM}). The experimental investigations were carried out in the State Key Laboratory of Coastal and Offshore Engineering at Dalian University of Technology (DUT), using the '6-D Measurement System' (6D-UMS) to obtain six degree of motions for both the tunnel and twin-barge. For the numerical study hydrodynamic properties were obtained from the diffraction/radiation potential code WAMIT for simplified tunnel and twin-barge elements and used to derive fully coupled motion behavior using the time-domain mooring simulation software OrcaFlex^{TM}. The results are presented in order to provide insights into the motion characteristics for the different configurations studied. The main findings indicate that the sway and roll motions for the coupled tunnel & twin-barge configuration decrease with increasing wave incidence angle and immersion depths. The use of additional mooring lines to restrain the tunnel element to the seabed played a further role in reducing the motions of the tunnel element, particularly when subjected to large amplitude and long period waves.

Keywords：Immersed tunnel；Coupled response；Regular waves；Twin-barge；Mooring system; Installation procedure

1. Introduction

Due to the growing economic developments, the increased demand for roads to cross seas has led to an increase in transportation construction. A new alternative to existing bridge or tunnel constructions are subsea constructions, installing tunnel elements on the seabed that have less visual impact and potentially shorter construction and installation time.

For large-scale undersea tunnel engineering, immersed tunnel elements have been widely used [1,2] because of the advantages gained due to availability of variable section shapes, adaptability to the seabed bathymetry, defined stress characteristics, low burial depth and operation safety. Submersible Elevating Platform (SEP), square barge, twin-barge, floating crane and floating box methods are popular construction principles for immersed

tunnel elements. Due to the inherent stability of multiple hull barges, the twin-barge method has been widely used in large-scale seabed tunnel projects.

During construction, the safe and controlled lowering of tunnel elements is one of the processes, which is most difficult to implement, and as a result requires a high level of technology to reduce risk of damage [3]. Many studies have focused on underwater interfacing, foundation treatment, seismic response and structure anti-seismic [4-6]. The motion response characteristics of immersed tunnel elements during installation is still not fully understood and further research is need to de-risk and advance installation methods. Jensen et al. [7] derived a tool for the Busan-Geoje tunnel project, enabling the motion characteristics of the tunnel element subjected to offshore wave loading to be studied. Toshio Aono et al. [8] carried out the numerical simulation and the experimental investigation on the stability of the Japanese NaHa immersed tunnel elements for different wave conditions, focusing on the effect of different bottom friction coefficients and ballast water weights on the sliding of the tunnel. Chen et al. [9] conducted a series of experiments to investigate the motion characteristics of an unmoored tunnel element subjected to irregular wave actions. Zuo et al. [10] conducted experimental studies on the motion behavior of the tunnel element being lowered by a single barge.

By using a twin-barge method for the transportation to the installation location and the consequent lowering and installation process, the symmetrical arrangement of two hulls provides a potential benefit allowing the suspended tunnel element to be adjusted in the transverse and longitudinal directions. However, during the installation processes environmental conditions (wind, wave and current) could result into excessive twin-barge motions that would affect the accurate control of the tunnel element during positioning and lowering procedures. Anchoring the tunnel and twin-barge to the seabed could provide additional stability and de-risk the installation procedure. The study presented here investigates the dynamic motion characteristics of a fully coupled tunnel & twin-barge configuration, considering additional mooring arrangements to constrain tunnel element motions during the installation procedure.

The investigation presented here describes initially the experimental and numerical approaches (section 2). Detailed information is provided to describe the experimental set-up and procedure as well as the numerical approach that was applied. Furthermore, a study is provided to derive the system properties (natural frequency and damping characteristics) essential for further response investigations. In section 3 the motion responses of the tunnel element and floating twin-barge are analysed. First, the experimental dynamic behavior of the tunnel-barge system is analyzed (herein the ‘tunnel-barge system’ refers to the configuration where the tunnel element is suspended by the twin-barge). Then, the effects of the twin-barge and the mooring system on the tunnel motions are investigated. Finally, the numerical simulation of the tunnel-barge system is carried out to validate the dynamic response of the tunnel element. The work is concluded in section 4 and future work has been identified.

2. Experimental and numerical approach

2.1. Experimental approach

2.1.1 Experimental set-up

The experiments were carried out in the ocean environmental flume of the State Key Laboratory of Coastal and Offshore Engineering at Dalian University of Technology (DUT). The wave flume is 50m long, 3.0m wide and 1.0m deep. A sketch of the 1:50 scaled experimental setup showing a moored twin-barge and the suspended tunnel element is shown in Fig. 1. The normal incident waves were generated from a piston-type wave maker at one site of the wave flume, with a wave absorbing beach covered with porous elements at the opposite site to

absorb wave energy and hence minimize wave reflection.

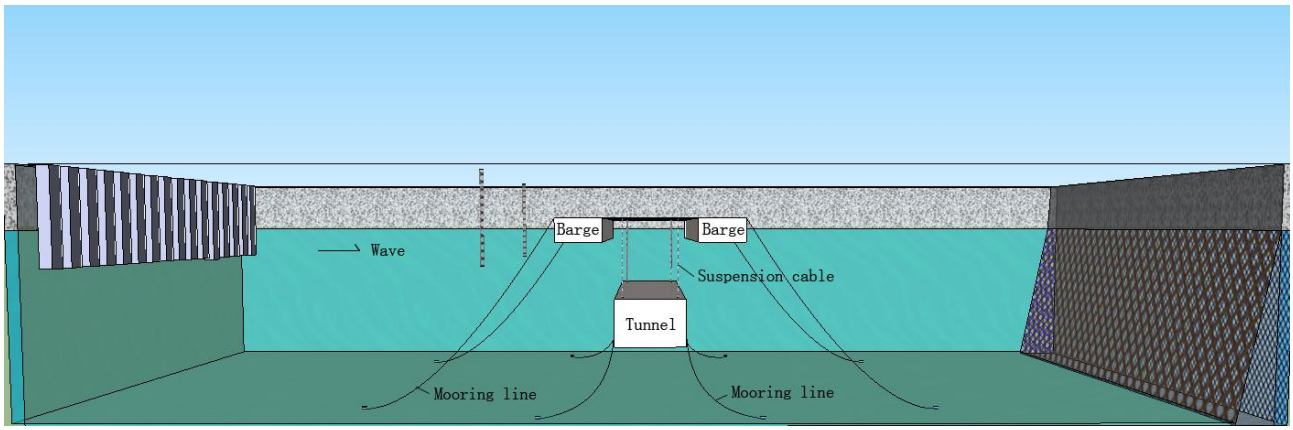

Fig.1 Sketch of the experimental set-up of moored twin-barge and suspended tunnel element

The tunnel-barge system consists of a twin-barge and tunnel element as shown in Fig. 1. Station-keeping of the tunnel element was achieved from the twin-barge using four suspension cables, as well as additional four mooring lines from the tunnel element to the tank floor. Furthermore, the twin-barge was kept on station with further four mooring lines anchored also to the tank floor. On the wave paddle side of the tunnel element, two wave height gauges were symmetrically positioned to provide real-time measurement of the wave surface. The experimental parameters used to study the motion characteristics of the suspended tunnel element in regular waves are listed in Table 1.

Table 1: Experimental parameters

Parameter(unit)	Nomenclature	Full scale	Model scale
Water depth(m)	*h*	40	0.8
Wave height (m)	*H*	1.5 - 2.5	0.03 - 0.05
Wave period (s)	*T*	5 - 8	0.7 - 1.1
Immersion depth (m)	*d*	10, 15, 20	0.2, 0.3, 0.4

2.1.2 Model preparation and experimental method

The scaled tunnel element was made of cement mortar covered with a protective polymer (fibre glass) layer to prevent water absorption of the tunnel element. The thickness of tunnel element wall was designed to provide appropriate weight of the model and end-cups were used to seal the element from potential flooding. A sketch of the immersed tunnel element model is shown in Fig. 2. The twin-barge model consisted of two hollow and airtight cuboid hulls made of polymer which were joined by a connecting steel frame. Iron blocks were fastened inside the barges to achieve the required heel and trim angles. A sketch of the tunnel element and the twin-barge are shown in Fig. 3 and the associated model parameters given in Table 2.

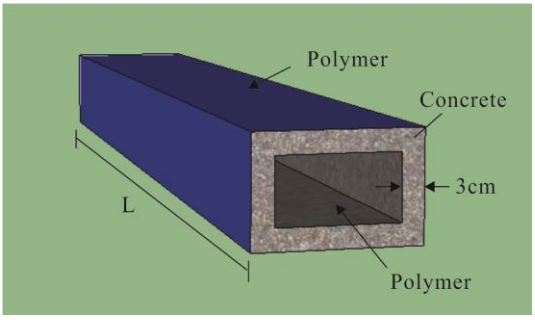

Fig. 2 Sketch of tunnel element model

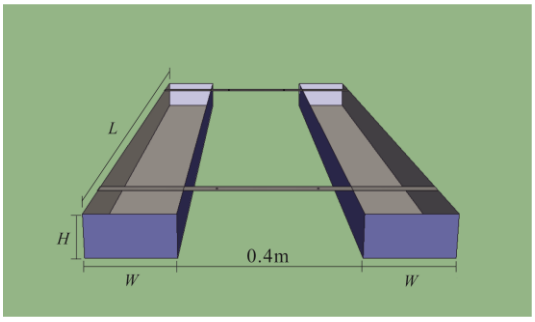

Fig. 3 Sketch of the twin-barge model

Table 2: Parameters of twin-barge and tunnel element model

Component	Parameter	Full scale	Model
Tunnel element	Length×Width×Height (m)	100×15×10	2×0.3×0.2
	Weight in water (kN)	1.47×10^{5}	1.176
	Negative buoyancy	2.08 %	2.08 %
Twin-barge	Length×Width×Height (m)	50×10×5	1×0.2×0.1
	Weight in air (kN)	2.16×10^{4}	0.173
	Draught (m)	2.75	5.5×10^{-2}

(Dimensions in Fig. 2 and 3 are at model scale)

The immersion depth and trim of the tunnel element can be adjusted by varying the length of the suspension cables. The suspension cable properties in respect to stiffness and weight were chosen carefully to provide scaled characteristics and additional mooring lines were included to the tunnel element to provide enhanced stability. In order to achieve the scaled mooring line properties only the Froude scale parameters were considered using weights and springs to adjust the weight and stiffness characteristics (see also Fig. 7). Similar the mooring stiffness and weight characteristics for both i) the four additional tunnel mooring lines and ii) the four twin-barge mooring lines, were adjusted using springs and weights to achieve Froude scaling properties.

Fig. 4(a) shows the anchor and fairlead attachment points with respect to the global coordinate system for all mooring lines and Table 3 provides the associated values. The local coordinate origins of tunnel and twin-barge were on the centroid of tunnel and the onshore side of the barge (left in front view), respectively. The origin point of global coordinate axis was the perspective point of the tunnel's centroid on the still water surface. The twin-barge mooring lines were aligned with the wave direction, whilst the tunnel element mooring lines were spread at 45°. The model scale mooring line properties for all twin-barge mooring, tunnel element mooring and suspension cable are given in Table 4.

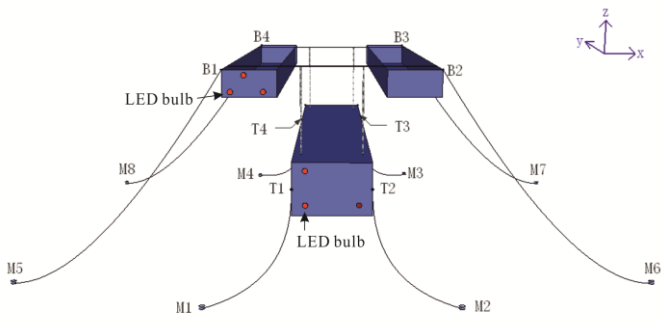

(a)

(b)

Fig. 4 Tunnel and twin-barge configuration: (a) mooring line coordinates (b) 6D-UMS configuration

Table 3: Coordinate of the attachment and anchor points of mooring lines

Attachment point	Global coordinate (m)	Local coordinate (m)	Anchor point	Global coordinate (m)	Local coordinate (m)
T1	(-0.15, -1, -0.1-d)	(-0.15, -1, 0)	M1	(-0.433, -1.283, -0.8)	(-0.433, -1.283, d-0.7)
T2	(0.15, -1, -0.1-d)	(0.15, -1, 0)	M2	(0.433, -1.283, -0.8)	(0.433, -1.283, d-0.7)
T3	(0.15, 1, -0.1-d)	(0.15, 1, 0)	M3	(0.433, 1.283, -0.8)	(0.433, 1.283, d-0.7)
T4	(-0.15, 1, -0.1-d)	(-0.15, 1, 0)	M4	(-0.433, 1.283, -0.8)	(-0.433, 1.283, d-0.7)
B1	(-0.1, -0.5, 0.04)	(-0.1, -0.5, 0.0475)	M5	(-1.55, -1, -0.8)	(-1.25, -1, -0.7925)
B2	(0.7, -0.5, 0.04)	(0.7, -0.5, 0.0475)	M6	(1.55, -1, -0.8)	(1.85, -1, -0.7925)
B3	(0.7, 0.5, 0.04)	(0.7, 0.5, 0.0475)	M7	(1.55, 1, -0.8)	(1.85, 1, -0.7925)
B4	(-0.1, 0.5, 0.04)	(-0.1, 0.5, 0.0475)	M8	(-1.55, 1, -0.8)	(-1.25, 1, -0.7925)

Table 4: Twin-barge and tunnel element mooring as well as suspension cable properties

Component	Immersion depth (m)	0.2	0.3	0.4
Mooring line of twin-barge	Length (m)		1.5	
	Weight (kg/m)		6.5×10^{-2}	
	Stiffness (N/m)		1.34×10^{3}	
Mooring line of tunnel element	Length (m)	0.7	0.62	0.54
	Weight (kg/m)		8.5×10^{-2}	
	Stiffness (N/m)	3.4×10^{3}	3.4×10^{3}	3.4×10^{3}
Suspension cable	Length (m)	0.24	0.34	0.44
	Weight (kg/m)		1.02×10^{-9}	
	Stiffness (N/m)	2.34×10^{3}	1.37×10^{3}	1.07×10^{3}

The motion response of the twin-barge and the tunnel element was obtained using an 'Untouched 6-D Measurement System' (6D-UMS) developed by DUT. Based on the principle of binocular vision, the measurement system used a dual lenses system to obtain characteristic target images simultaneously providing the advantage of being simple, non-intrusive and allowing high precision. Post-processing of the data to obtain model motion and provide data storage was carried out using a PC console. The 6D-UMS and the tunnel model are shown in Fig. 4(b).

The ray tracing method was applied to obtain the target position from the binocular vision measurements. The location of the 6D-UMS was at the exact front of tunnel element and twin-barge models, with the distance being around 0.5m between the dual lenses of the 6D-UMS and the target images on the tunnel-barge system. The original positions of both tunnel element and twin-barge were recorded by the dual lenses to calculate the correlation coefficients in the system before testing. The correlation coefficients related to the relative location of the dual lenses and the target points should be less than the system permissible error of 0.01%. Hereby, the location of the 6D-UMS cannot be moved during the experimental tests once the correlation coefficients of the original position were determined. The distance between the two lenses has a direct influence on measurement accuracy and range. The large relative position of the dual lenses will improve the accuracy of the 6D-UMS, but will decrease the measurement range. The distance between the two central points of dual lenses was set at 6.5cm in the experiment.

Three non-collinear LED bulbs were used as signature points on the external surface of both tunnel and twin-barge (Fig.4 (a)). The measured motion components of tunnel and barge were calculated by the variation of position of the signature points. Due to the different refractive index of light in different media (water and air), it

was important that the target signature points remained in one medium. This was of importance for the twin-barge, where due to wave actions the LED bulbs potentially could emerge out of the water, which could affect the accuracy of the measurements and distort the results. The precision of the translation motion (sway, heave and surge) of the 6D-UMS can be achieved to be less than 0.3%FS, and for rotation (roll, pitch and yaw) the error was less than 1.2%FS. The sampling rate of the real-time measurement system was 30Hz. The wave surface elevations were measured using a conductive system DLY-1 Wave height measuring system, developed by DUT. The measurement range of wave height of this system is 0 - 30cm, and the absolute error is less than l mm. The regular wave conditions used in this study are shown in Table 5.

Table 5: Regular wave conditions used for study

Test I.D.	Immersion depth *d*(m)	Wave height *H* (m)	Wave period *T* (s)
T_01	0.3	0.05	0.7, 0.85, 1.0, 1.1
T_021	0.2	0.04	0.7, 0.85, 1.0, 1.1
T_022	0.2	0.05	0.7, 0.85, 1.0, 1.1
T_031	0.3	0.03	1.1
T_032	0.2, 0.3, 0.4	0.05	0.7, 0.85, 1.0, 1.1
T_04	0.4	0.05	0.7, 0.85, 1.0, 1.1

2.2 Numerical approach

In order to provide additional information about the experimental study a numerical analysis was performed to predict the complex coupled behavior of the system using a commercial fully dynamic simulation software Orcaflex ™. Initially the hydrodynamic properties of the tunnel element and twin-barge were calculated by the diffraction/radiation potential code WAMIT, using a boundary element mesh method for each of the 6 degrees of freedom of the tunnel and twin-barge model. Matlab was used to calculate the geometric mesh of both the tunnel and twin-barge, utilizing the symmetry of these geometries about the *x*- and *y*-axis. Only the submerged geometry (at equilibrium) was considered, and hence not the steel frame which connects the two hulls (Fig. 5). For the numerical calculation of the hydrodynamic frequency-dependent data, the values of radiation damping, added masses, the load Response Amplitude Operators (RAOs) and the associated phases at the metacenter at the equilibrium position of the tunnel were calculated in a similar approach as described by Harnois et al. [11]. The hydrodynamic loads on the mooring system were calculated using an extended form of Morison's Equation [12], as the wave diffraction force can be ignored when the ratio of principal body dimension to wavelength is less than 0.2. The mooring line drag coefficients were taken from the Orcaflex™ manual [13] for the chains and from DNV standards [14] for the ropes.

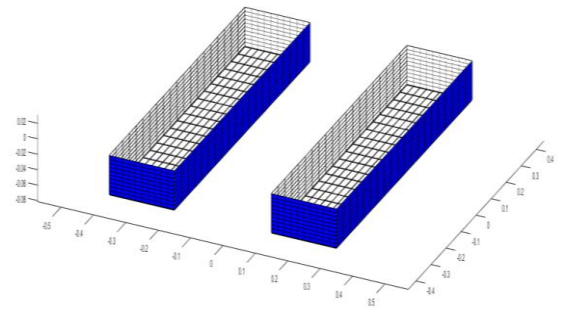

Fig. 5. Twin-barge mesh used for the diffraction/radiation potential analysis

For the numerical simulation the 1:50 scale tank configuration was created as a 3D model within OrcaFlex^{TN}, including mooring and suspension line arrangements (Fig. 6). The truncated twin-barge and tunnel element mooring lines and suspension cables were simplified and scaled (Table 6). The mooring number index represents the mooring line of the tunnel element, the suspension cable, and twin-barge, respectively. The added mass coefficients of the mooring chains were taken from the classification of mooring systems for Permanent Offshore Units [15]. The suspension cables for the numerical model were simulated as polypropylene rope (8-strand multiplait), with studlink chain used to represent the appropriate weight and axial stiffness of the mooring lines of both tunnel element and twin-barge, four mooring lines of the tunnel element orientated facing the wave symmetrically (Fig. 6).

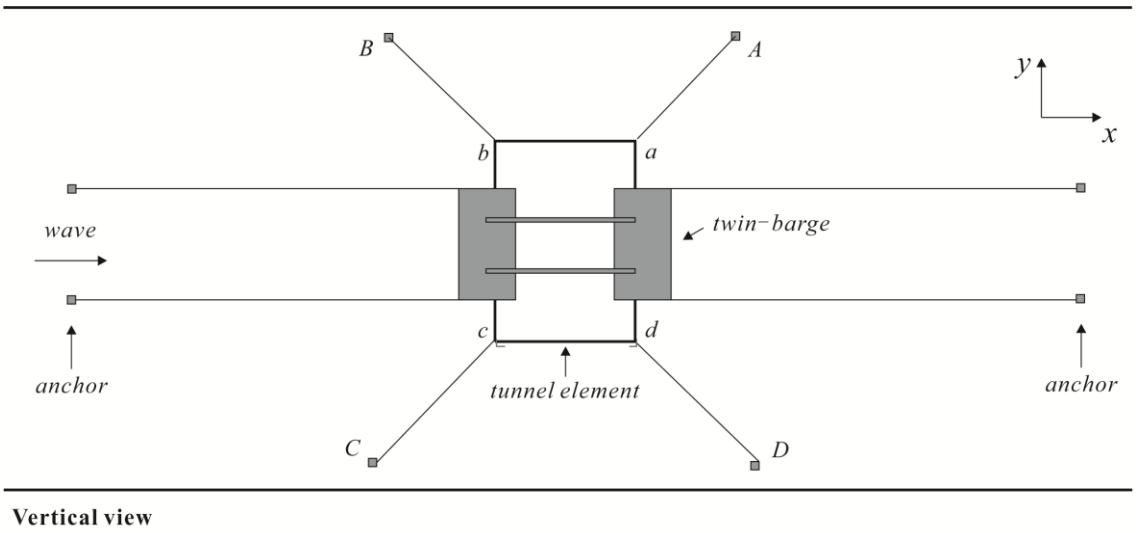

Fig. 6 Schematic of vertical view of the numerical model

Table 6: Properties of the simplified mooring system and suspension cables (Cd_a and Cd_n are axial and normal drag coefficients)

Mooring number index	Simplified line type	Nominal diameter (m)	Mass (kg/m)	Axial stiffness (EA, N)	Added mass coefficient	Drag coefficient	
						Cd_a	Cd_n
1	Chain	0.004	8.76×10^{-2}	3.4×10^{3}	0.5	0.4	1
2	Rope	0.002	1.02×10^{-3}	2.38×10^{3}	0	0.008	1.2
3	Chain	0.003	6.15×10^{-2}	1.34×10^{3}	0.5	0.4	1

In order to achieve a representative simulation model of the experimental set-up it was essential to introduce Froude-scaled spring components and also to simulate the behavior of the load transducers that provide an additional mode characteristic. Initial calibration without introduction of these two elements resulted in significant errors and hence for all results presented the spring and transducer properties are considered.

The twin-barge and tunnel element mooring lines, as well as suspension cable are simulated using a discretized method with segments representing the spring and damping properties, and nodes representing the mass of the line segments. The Lumped-mass method was used in the numerical model to calculate the mooring line tension and the suspension cable force. All mooring lines and suspension cable were discretized into 20 equal segments connecting 21 node points. The mooring line node indexing starts at the seabed anchor point (given

an index of 0), and the midpoint of the segment between the node i and node i+1 was given an index of i+1/2. Each discretized segment of the mooring lines has identical parameters of density, volume-equivalent diameter, Young's modulus, unstretched length, and internal damping coefficient. The mooring line model combines damping loads and internal stiffness with buoyancy loads, weight, hydrodynamic loads and contact loads with seabed and tunnel-barge system. The model calculates the hydrodynamic loads at the segment midpoints and then distributing them to the node points [16-17]. Morison's equation was used to calculate the added mass and axial drag of mooring chains. The simulation model approach is indicated in Fig. 7.

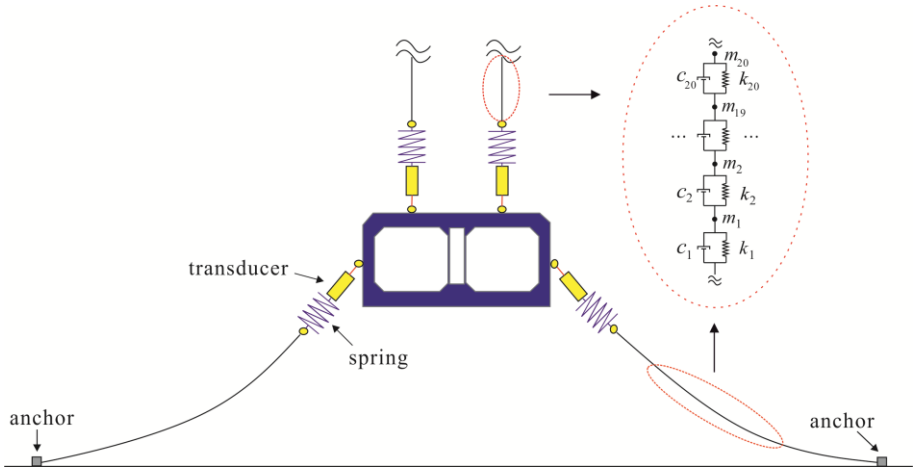

Fig. 7 Schematic of analysis approach

The incident waves propagate along the flume in the positive x direction (along the width (sway) of the tunnel element). Wave-current interaction and bottom dissipation are not included in this numerical simulation. The center of gravity (COG) of the experimental twin-barge in free-floating conditions was at 0.025m below the static water lever in the flume. The same draft of twin-barge was set in the numerical model. The relative parameters and the main properties of tunnel-barge system in the numerical model are given in Table 7.

Table 7

Properties of full scale and model tunnel element and difference with theoretical values.

	Full scale values	Measured scaled values	Theoretical scaled values	Relative error
Mass of tunnel (t)	1.53 x 10^4	0.1225	0.1225	0%
Moment of inertia I_{xx} (t m^2)	1.28 x 10^7	0.043	0.041	4.65%
Moment of inertia I_{yy} (t m^2)	4.15 x 10^5	0.0014	0.0013	7.14%
Moment of inertia I_{zz} (t m^2)	1.3 x 10^7	0.045	0.042	6.67%

2.3 Decay test

To study the resonance mechanisms of the tunnel-barge system under wave actions, decay tests of the tunnel and twin-barge in still water were also carried out and simulated using the numerical model. This was achieved by applying an offset to the twin-barge from its equilibrium position for each degree of freedom and measuring the decaying response of both the twin-barge and tunnel element with the 6D-UMS. As the tunnel element was connected to the twin barge through the suspension cables decaying motion could be achieved through an offset and release of the twin-barge. Prior to decay tests the wave disturbance was kept to a minimum.

In order to study the natural frequencies and damping properties, experimental decay tests were performed

for three different set-ups; i) twin-barge and its mooring only, ii) tunnel element suspended form a fixed platform, and iii) coupled tunnel-barge configuration with twin-barge mooring (but with no tunnel element mooring). For decay test set-up iii), coupled tunnel-barge configuration with twin-barge mooring, only the tunnel element motion was recorded. For the case of the tunnel element without mooring, the restoring force of tunnel mooring is zero, but that for the mooring lines of the twin-barge are not zero. Fig. 8 shows a result of the decaying sway motion for the tunnel element and twin-barge only, as well as for the tunnel-barge system. An additional study has been implemented to obtain the natural frequency for the fully coupled tunnel-barge system, including the tunnel element mooring. In the experiment, repeated decay tests were conducted for each case and the free vibration frequencies of the tunnel element, twin-barge and tunnel-barge system were evaluated by averaging the measured decaying motions. Due to the sudden release of the mooring system, the additional damping may influence the decay motions of the tunnel and twin-barge and consequently the first decay oscillation was ignored for evaluation. For the tunnel element and twin-barge decay tests, five consecutive troughs and peaks were used to evaluate the damping coefficients and free vibration period. The natural frequencies of the tunnel element and twin-barge in still water are given in Table 8. The natural frequencies where obtained to provide a relation to the wave excitation frequencies. Comparing natural frequencies and wave excitation frequencies for the different scenarios it can be identified that the roll motions for tunnel-barge system and heave motions for the twin-barge have corresponding frequencies causing potential resonance modes. For the other cases the natural frequencies are sufficiently different from the wave excitation frequencies studied and hence resonance is unlikely. However the twin-barge and tunnel element roll natural frequencies are close to the wave excitation frequencies.

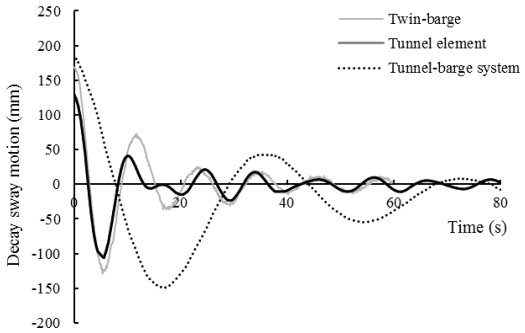

Fig. 8 Sway decay test for the twin-barge and tunnel element motions (d=0.4m)

Table 8: The free vibration frequency of the tunnel and twin-barge in static water

Test conditions	Sway (Hz)		Heave (Hz)		Roll (Hz)	
	experiment	numerical	experiment	numerical	experiment	numerical
Twin-barge	0.088	0.087	1.06	1.02	0.59	0.57
Tunnel element (without mooring lines)	0.090	0.089	0.26	0.24	0.76	0.74
Tunnel element (with mooring lines)	--	0.10	--	0.28	--	0.66
Tunnel-barge system (without mooring lines)	0.027	0.027	0.41	0.39	0.87	0.90
Tunnel-barge system (with mooring lines)	--	0.03	--	0.36	--	0.93

2.4 Pretension

The pretension of the mooring lines in the numerical model were calculated by Catenary method for static and quasi-static modes, and the bend stiffness effect are ignored to find the equilibrium position of the mooring lines. According to the principle of statics, the mooring line pretension relative to the mooring line weight,

buoyancy, axial elasticity, and seabed touchdown length. The diagrammatic sketch of the simplified calculation of mooring line tensions is shown in Fig. 9.

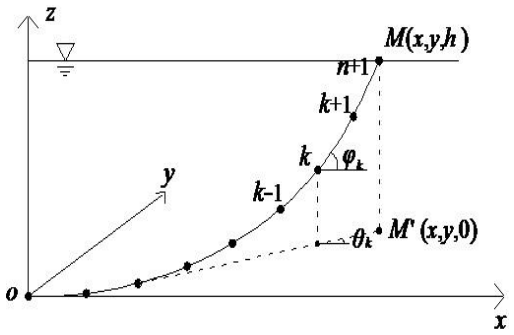

Fig. 9 Sketch of the simplified calculation model of the mooring lines

The static equilibrium equation on the *k*-node is established as below:

$$\begin{aligned} &X \text{ direction:}\quad T_k \cos\varphi_k \cos\theta_k = T_{k-1} \cos\varphi_{k-1} \cos\theta_{k-1} \\ &Y \text{ direction:}\quad T_k \cos\varphi_k \sin\theta_k = T_{k-1} \cos\varphi_{k-1} \sin\theta_{k-1} \\ &Z \text{ direction:}\quad T_k \sin\varphi_k = T_{k-1} \sin\varphi_{k-1} + W\bar{l} \quad (k = 2,3\ldots,n) \end{aligned} \tag{1}$$

where θ_k is the angle between the projection of the *k*th segment on the plane *xoy* and the *x-axis*, φ_k the angle between the projection of the *k*th segment on the plane *xoy* and the *k*th segment, T_k the tension between the *k*-node and *k*+1 node, *W* the mass of the unit length of chain in water, the initial length between the adjacent nodes.

The mooring line tensions can be obtained from the following equation:

$$\begin{aligned} X_m &= \sum_{k=1}^{n} l_k \cos\varphi_k \cos\theta_k = \bar{l} T_x \sum_{k=1}^{n} T_k^{-1} + k\bar{l} T_x / (EA) \\ Y_m &= \sum_{k=1}^{n} l_k \cos\varphi_k \sin\theta_k = \bar{l} T_y \sum_{k=1}^{n} T_k^{-1} + k\bar{l} T_y / (EA) \\ Z_m &= \sum_{k=1}^{n} l_k \sin\varphi_k = \sum_{k=1}^{n} \left[\bar{l}(1 + T_k / EA) \cdot kW\bar{l} / T_k \right] \end{aligned} \tag{2}$$

in which T_{xy} is the projection of T_k on the plane *xoy*, and $T_x = T_{xy} \cdot \cos\theta_k$, $T_y = T_{xy} \cdot \sin\theta_k$, l_k the length of the *k*th segment, *E* the elastic modulus of the chain, *A* the equivalent sectional area of the chain.

3. Experimental and Numerical results

3.1 Experimental results

3.1.1 Effect of twin-barge movement on the motion response of the tunnel element

In the following discussion of the results only the sway, heave and roll motions of the tunnel element are considered under the normal incident wave actions. The typical time history of the motion response of the tunnel-barge system with *H*=0.05m, *T*=1.1s and *d*=0.2m are shown in Fig. 10. It can be observed that the motion response of the tunnel element suspended from twin-barge exhibits strong nonlinear characteristics when positioned at the lower immersion depths. The large nonlinear tunnel motions are likely to be caused by the coupled interactions with the twin-barge, which experienced strong dynamic response with water splashing on the deck of barge in the experiment. The heave tunnel motions are not symmetrical relative to its equilibrium position, the upper tunnel motion amplitudes are slightly larger than that of the downward movement. This may be caused by the upward force provided by the suspension cables acting on the tunnel element when it moves downwards.

Conversely the suspension cables are slack when the tunnel element moves upwards.

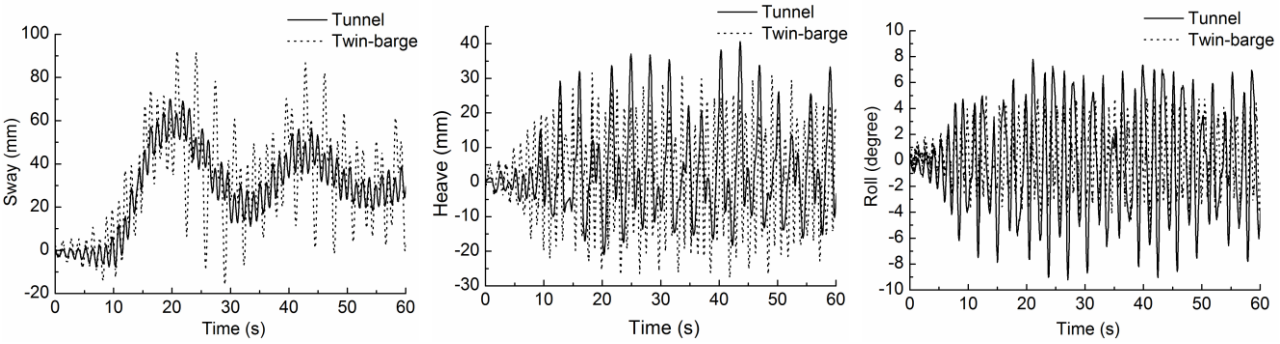

Fig. 10 Typical time history of the motion response of tunnel element suspended from twin-barge (d = 0.2m, H = 0.05m, T = 1.1s)

In order to discuss the influence of the twin-barge on the motion of the tunnel element a comparison is made between the respective responses of the tunnel element suspended by the twin-barge and also a fixed platform in test T_01. The mooring system parameters for the tunnel element suspended from a platform were kept consistent with the mooring line parameters shown in Table 5. Fig. 11 provides a comparison of the motion response of the tunnel-barge and fixed platform for different wave periods and a wave height of H = 0.05m. The observation can be made that the tunnel-barge system results in a larger roll response of the tunnel in comparison to the fixed platform arrangement. However, for sway and heave the tunnel element undergoes larger motion response for the fixed platform configuration, which is likely to be due to the higher natural frequency of the twin-barge. The roll natural frequencies of the tunnel-barge system are closer to the wave excitation frequencies compared to fixed platform arrangement and this results in larger responses for the tunnel-barge system.

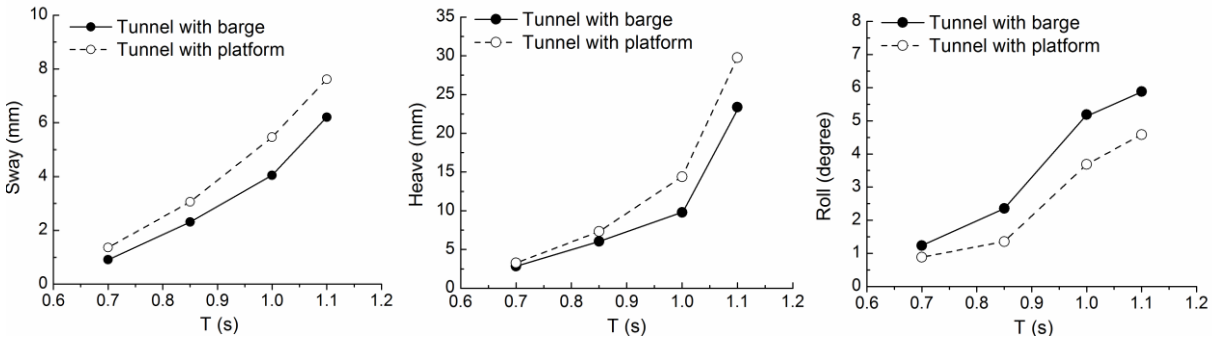

(a) (b) (c)

Fig. 11a-c Comparison of the tunnel element motions for tunnel-barge system and fixed platform arrangement (H = 0.05m, d = 0.3m)

3.1.2 Effect of tunnel mooring lines on the motion response of the tunnel element

To study the influence of tunnel mooring lines on the response of the tunnel element for the tunnel-barge system, a range of tests were conducted with and without tunnel element mooring lines. The tunnel element motion responses were compared for tests T_021 and T_022 (table 5); for d = 0.2m and H = 0.04 and 0.05m.

The resultant response modification of the tunnel element are shown in Fig. 12a-f for sway, heave and roll. Figs. 12a-c show the RAOs for the three modes and Figs. 12d-f present the percentage difference between the two case (with and without tunnel element mooring line). The RAOs (Response Amplitude Operator) in Fig.12 and Fig.16 is a dimensionless parameter relative to the ratio of the motion amplitude and the wave height component.

Whereby the percentage difference $\Delta\delta$ is expressed in the form:

$$\Delta\delta = ((\delta_{without} - \delta_{with})/\delta_{without}) \times 100\% \quad (3)$$

It can be observed that in sway and roll the addition of the tunnel element mooring line reduces the motion characteristics between 5% and 25%, (although this is dependent on the incident wave period and motion mode, see Figs. 12d,f). Conversely, the motion response in heave increases when the tunnel element mooring lines are added. An increase between 5% to 20% can be observed related to wave height and wave period. Yang et al. [18] explained this phenomenon to be the result of having two spring systems (with the upper spring provided through suspension cable and lower spring provided through the tunnel element moorings) that are acting on the tunnel element in the heave motion. As a consequence the amplitudes of the tunnel element heave motion increase when the tunnel element mooring lines are attached. This agrees with the results obtained by Chen et al. [19] for the case of increasing the negative buoyancy of the tunnel element. Furthermore, the maximum motion amplitude of the tunnel element with the largest wave height against different wave periods are mostly larger than that of lower wave height, the maximum difference of the tunnel motions (with and without mooring lines) are larger with the large wave height conditions in sway, heave and roll modes.

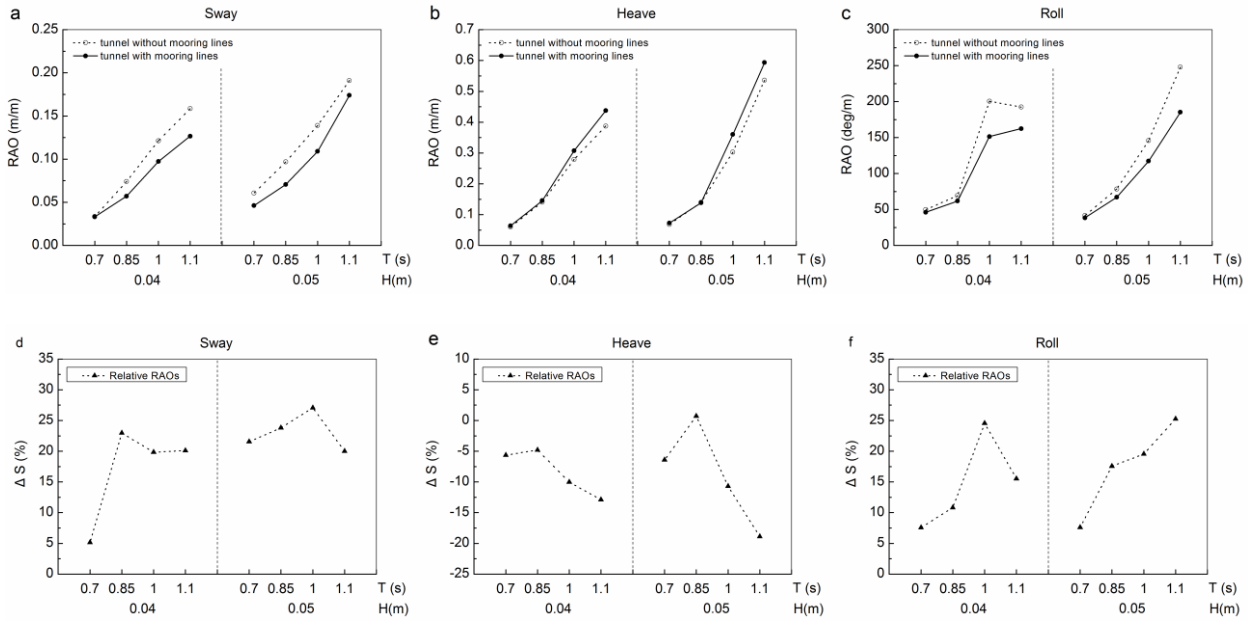

Fig. 12a-f Comparison of the tunnel element motions for tunnel-barge system with and without tunnel mooring lines (H = 0.04m and 0.05m, d = 0.2m)

3.1.3 Motion characteristics of tunnel element suspended by the twin-barge

In the following section results are presented for the tunnel-barge system which comprises both the twin-barge and tunnel element mooring lines. Figs. 13(a)-(c) compares the time series of motion response for the tunnel element and the twin-barge for test case T_031 (d = 0.3m, H = 0.03m, T = 1.1sec). In order to observe the simultaneous movement of tunnel and twin-barge more clearly, the time series from 20s to 30s for each mode are enlarged in Figs. 13(d)-(f). It can be seen that the motion period and phase of tunnel element in the sway direction are synchronized and are consistent with the twin-barge. In the heave and roll modes there is a phase difference between tunnel and twin-barge, that could be the cause of a delayed reaction force caused by the suspension cables to the tunnel element.

In respect to amplitude magnitudes it can be observed that the sway and heave motion responses of twin-barge are larger than that of the tunnel element. For the roll motion, however, the tunnel element exceeds the twin-barge motion. It can be observed that the twin-barge has some higher frequency modes in addition to the wave response mode that could be the result of inertia loads caused by the coupled action between tunnel element and twin-barge transmitted via the suspension cables. Also it can be observed that the roll motion of twin-barge is less than that of the tunnel element, again a possible explanation could be that the coupled interaction of tunnel element and twin-barge feature varying one-sided tension loads which cause larger excitation to the tunnel element.

As shown in Fig. 13(a), slow-drift forcing also influences the sway motions of the tunnel element. The slow varying sway motion can alter the pre-tension of both the tunnel element and twin-barge mooring lines, consequently changing the natural frequencies of the tunnel-barge system, and hence causing different response characteristics. The complexity of motion response is further complicated through the variation in stiffness characteristics of the mooring lines and therefore the irregular motion responses, for most tunnel element and twin-barge response modes, could be attributed to this phenomena.

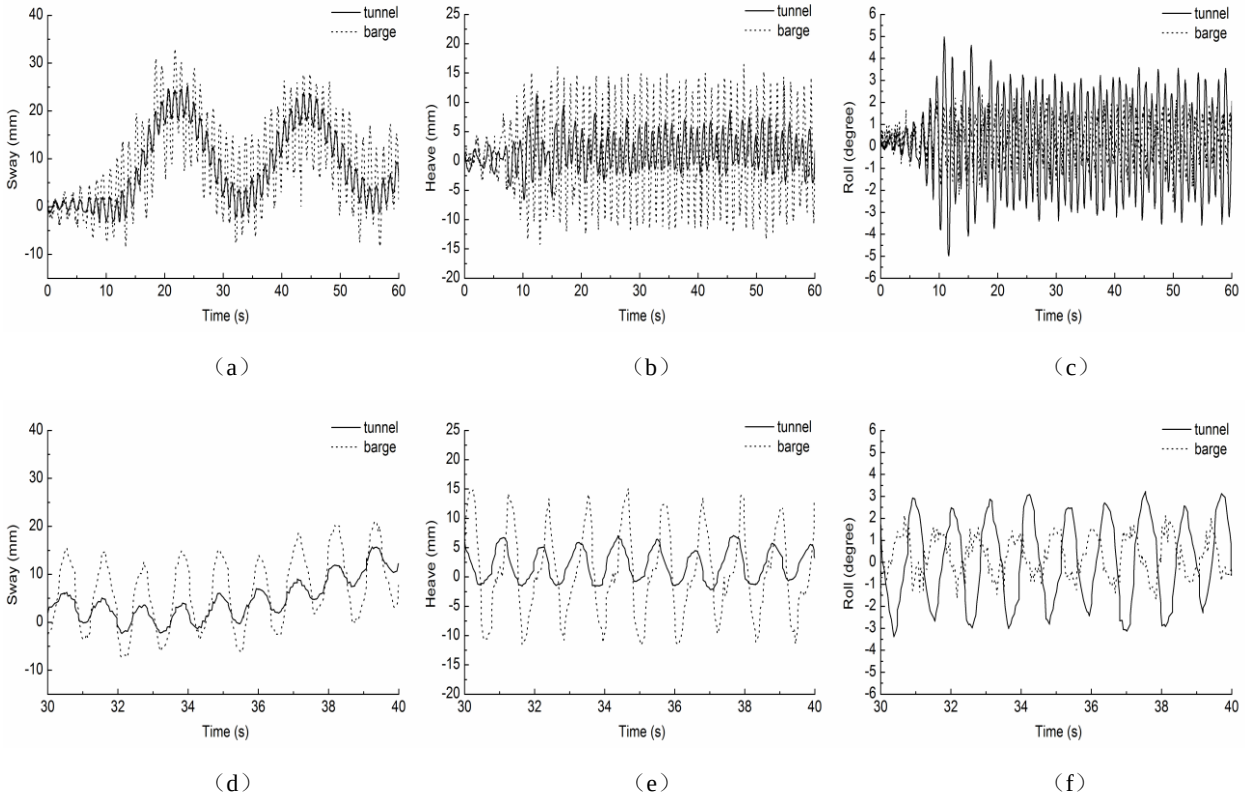

Fig. 13a-f Time series of motion responses of moored tunnel element suspended by twin-barge (test T_031)

In order to explore the tunnel-barge system coupled dynamic behavior in regular waves, the motion response of the tunnel-barge system with the measured suspension cable force are shown in Fig. 14. In the Figure, the left y-axis represents the motion response of the tunnel element and the twin-barge, while the y-axis on the right side represent the recorded suspension cable loads. It can be observed that there is a phase difference between the onshore and offshore side suspension cable tensions and the heave and roll motions. The suspension cables exhibit alternate slack phenomenon, this is likely to be caused by the large dynamic response of the tunnel element in roll direction, which could also explain the different motion periods and phases in the tunnel-barge system. These results suggest that the complicated phase relation between the suspension cable tensions and the complexity of

motion response in the tunnel-barge system is due to the strong nonlinear interaction of the tunnel element with the twin-barge in waves.

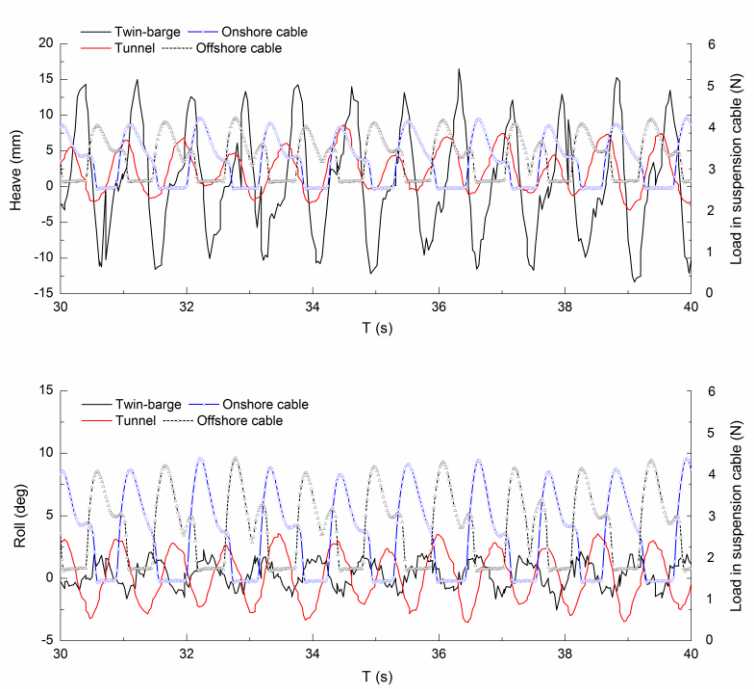

Fig. 14 Comparison of detailed motion responses of tunnel-barge system and suspension cable tensions (test T_031)

The fast Fourier transform was applied to the time series of tunnel motions in Fig. 13 for frequency spectral analysis. The frequency spectral results in Fig. 15 directly show the main frequencies of the tunnel motions in sway, heave and roll. It can be observed that there are two peaks on the sway displacement spectra, and only one dominant peak can be observed for the heave and roll motion spectra. Taking the sway motion as an example, the frequency of the two extreme value points on the amplitude spectrum curve in Fig. 15(a) are 0.045Hz and 0.9Hz. The higher frequency corresponds to first-order wave induced motions. The dominant frequency of the other component is 0.045Hz, which is the low frequency motion. The corresponding period is 22s and it can also be observed from the time series of sway motions in Fig. 13.

It can be identified from the spectral analysis of heave and roll (Fig. 15(b), Fig. 15(c)) that the dominant motions of tunnel element and twin-barge are at the first-order wave frequency. Furthermore, it can be observed that the heave motion amplitude of the tunnel element is smaller compared to the twin-barge, whilst for the roll motion the tunnel element exceeds the twin-barge motion amplitude.

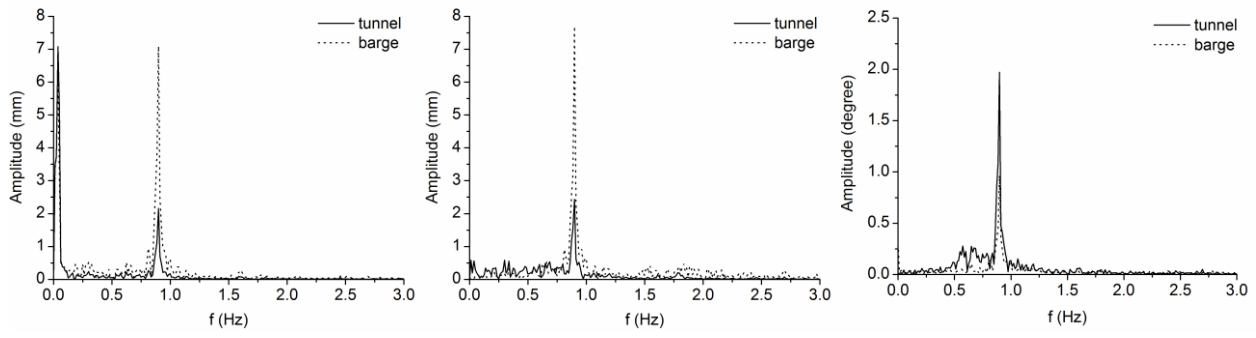

（a）sway　　（b）heave　　（c）roll

Fig. 15 a-c Frequency spectral of motion response of moored tunnel element suspended by twin-barge (test T_031)

Figs. 16a-f shows the RAOs of the tunnel element as well as the percentage difference for different immersion depth and for a range of wave periods with a wave height of H = 0.05m (see Table 5; T_032). The percentage difference $\Delta\delta$ is calculated using equation (3), where the immersion depth d = 0.2m is used as a reference case. The motion responses are presented for sway low frequency motion (Fig 16a) and sway (Fig 16b), heave (Fig 16c) and roll (Fig 16d) wave frequency motions. The corresponding percentage differences are shown in Figs. 16e-g, respectively.

It can be seen from Fig.16 that the RAOs of the tunnel element decrease with increasing immersion depth, particularly for the sway low-frequency mode. The percentage difference for the sway low frequency mode $\Delta\delta_{S\_low}$ between d = 0.2m and 0.4m is of the order of 80% to 135%, whilst the $\Delta\delta_{S\_low}$ between d = 0.2m and 0.3m is of the order of 30% to 70%. The sway wave frequency mode is increasing for larger wave periods. The percentage difference $\Delta\delta_{S\_wave}$ is negative identifying a decrease in response amplitude and at the order of -65% to -20% (d = 0.2m vs 0.4m) and -50% to -5% (d = 0.2m vs 0.3m), respectively. As for the sway wave frequency mode, for amplitude motion for heave and roll increase with larger wave periods. The percentage difference for both, heave $\Delta\delta_{H\_wave}$ and roll $\Delta\delta_{R\_wave}$, are smaller in magnitude compared to the sway mode ($\Delta\delta_{H\_wave}$ = -45% to -10% (d = 0.2m vs 0.4m), ($\Delta\delta_{H\_wave}$ = -35% to 10% (d =0.2 vs 0.3m); $\Delta\delta_{R\_wave}$ = -35% to -3% (d = 0.2m vs 0.4m), $\Delta\delta_{H\_wave}$ = -20% to 10% (d =0.2 vs 0.3m)).

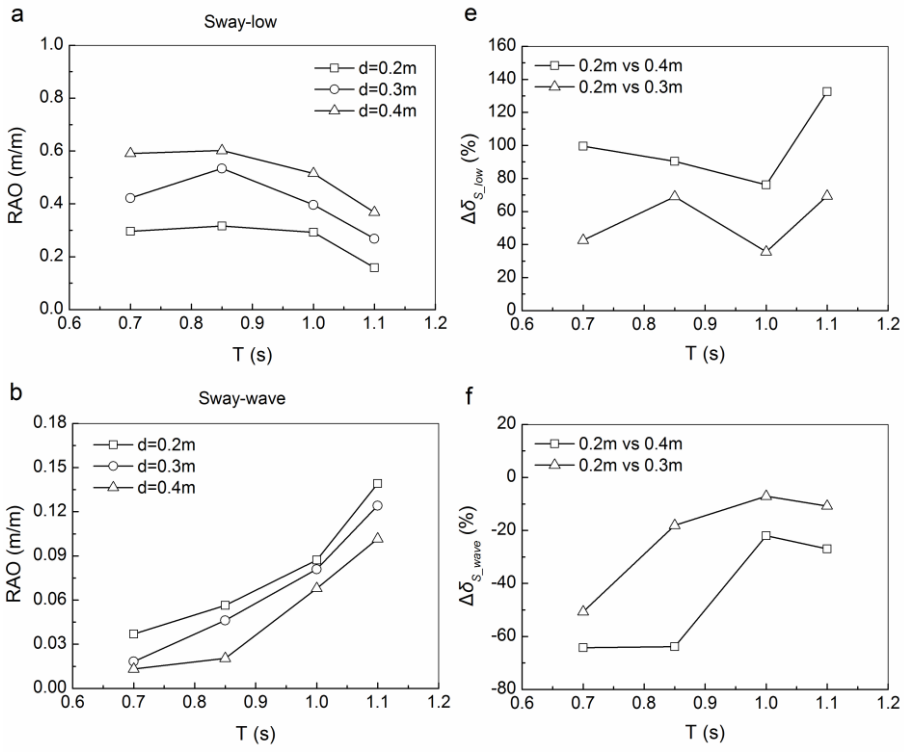

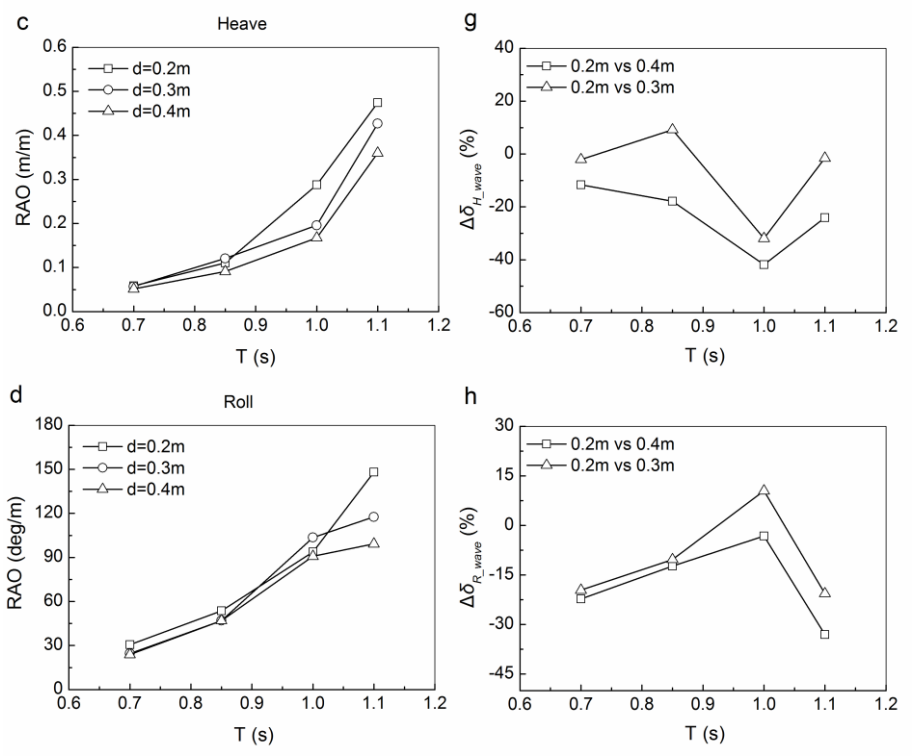

Fig. 16a-h The RAOs and of the tunnel element with different immersion depths and H = 0.05m: a) sway low frequency motion, b) sway wave motion, c) heave wave motion, d) roll wave motion; e) – g) corresponding percentage difference $\Delta\delta_{S\_low}$, $\Delta\delta_{S\_wave}$, $\Delta\delta_{H\_wave}$, $\Delta\delta_{R\_wave}$

3.2 Numerical tests

A preliminary numerical study was carried out based on the regular wave tests to allow a comparison between experimental results and numerical modelling. These tests correspond to sinusoidal waves with heights ranging from 0.03m to 0.05m and periods from 0.7s to 1.1s for three immersion depths (d=0.2m, 0.3m and 0.4m). The numerical simulation were run for approximately 60 waves to observe the steady motion response of the tunnel-barge model. The free surface elevations from the numerical model and experimental tests (measured at 50Hz) for H= 0.03m and T= 1.1s are presented in Fig. 17.

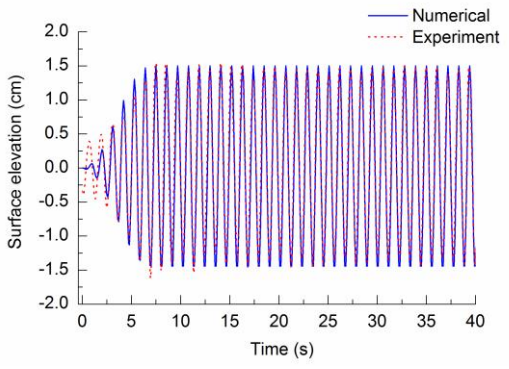

Fig. 17 Comparison between the experimental and numerical wave elevation

Fig. 18 provides a comparison of the numerical simulation and measured motion time series of both twin-barge and tunnel element for test T_031. In order to observe the steady response of the tunnel element, the motion history from 10s to 30s was chosen for the comparison in order to avoid initial transient behavior. With the

near-field wave conditions determined by the numerical modelling, the heave and roll motions are accurately replicated for the tunnel element and the twin-barge. Some differences can be seen in the sway direction, due to differences in the drift motion caused by second-order waves. In the example shown in Fig. 18 (a) and (d), the twin-barge is reaching nearly the same minimum sway position, while large differences can be observed between 38s < t < 40s with corresponding correlation coefficients greater than 0.3. For the tunnel sway motion, the minimum sway position is equal to -2.24m in the experiment and -0.18m in the numerical model. Despite these differences, the correlation coefficients are always larger than 0.43 for the sway motion.

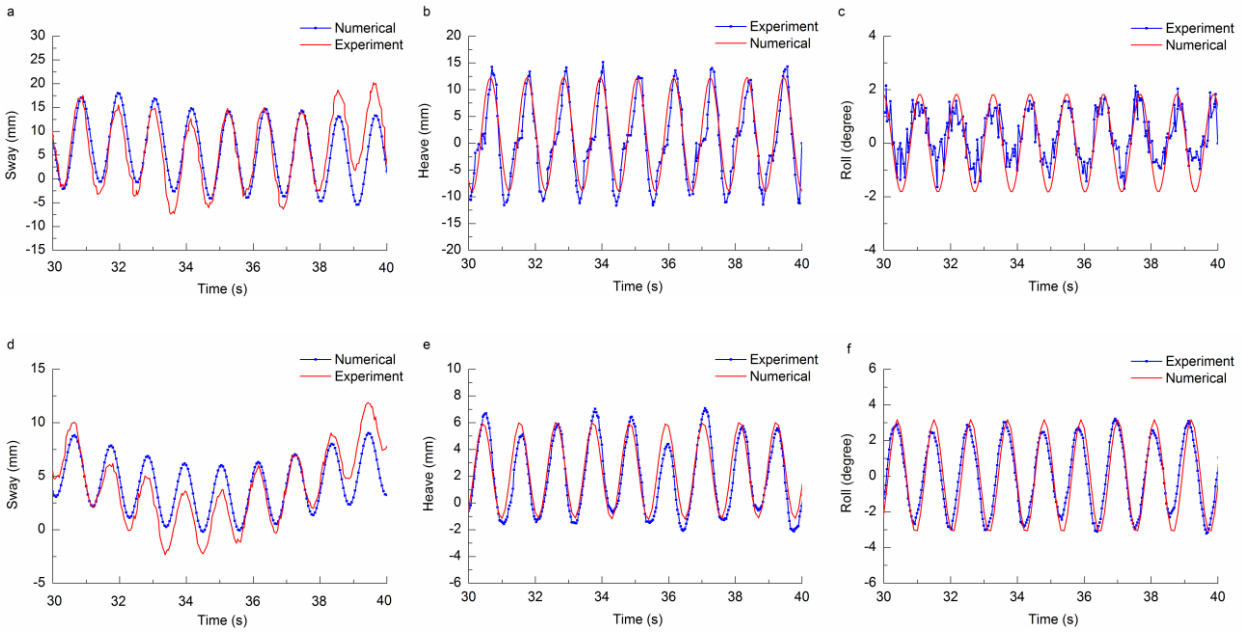

Fig. 18 Comparison of the motion time series of the twin-barge and the tunnel element between numerical simulation and experimental data for test T_031

Fig. 19 shows a comparison of the maximum values of the sway, heave and roll motions of the tunnel element for the case T_04 between the tank tests and the numerical model. The maximum tunnel motions are the maximum motion amplitude in each degree of freedom of the tunnel element. In the sway direction, only wave frequency motion (first-order waves) was considered to evaluate the tunnel dynamic response in the numerical model, hence the experimental low frequency component was separated from the sway motion of the tunnel element to fit the modelling results. The relative error is given by R= ((S_N - S_E) /S_E)x100% where S_N and S_E are the values obtained from the numerical model and experimental tests, respectively. In the case of test T_01, the mean relative error of the sway, heave and roll motion of the tunnel element is 1.44%, 3.11% and 2.81%, respectively. Based on the above analysis, the calculated motion response of the tunnel element in sway, heave and roll directions correspond well with the tank test results. Accordingly, it is concluded that the numerical model can be used in the dynamic analysis of the tunnel element suspended by twin-barge in waves.

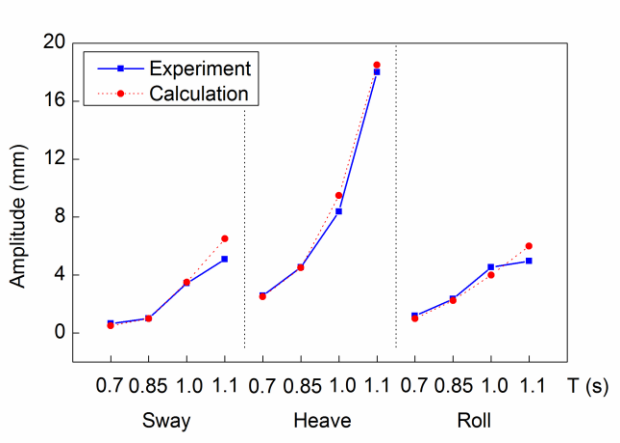

Fig. 19 Comparison of the maximum values of the tunnel motions between the numerical and experimental data (test T_04)

In Fig. 20, the motion amplitude of the tunnel element is presented for different wave incidence angles for regular waves of T=1.1s and H=0.02-0.05m. The results showed that the tunnel sway and roll motions decrease with the increasing wave incidence angle and decreasing wave height. The influence of wave height on the tunnel motions is relatively large for small angles of wave incidence. This is due to the fact that the tunnel element experiences more severe dynamic response with more energetic wave loading (at small incidence wave angles). The variation of heave tunnel motions is slight because the vertical wave force component which acts on the tunnel element is unvarying for the conditions studied (Fig. 20(b)). Furthermore, a point worth mentioning is that the roll motion amplitude of the twin-barge is less than that of the tunnel element, as shown in Fig.20(c). This could be due to the inherent stability of the twin-barge floating structure and the increased dynamic response of the tunnel element due to the movement of the twin-barge which has been discussed in section 3.1.1. Therefore, it is imperative that in order to reduce operational risks, tunnel roll motion control or mitigation needs to be considered in conjunction with the identification of an appropriate mooring system during the planning of construction procedures for this method of tunnel element immersion.

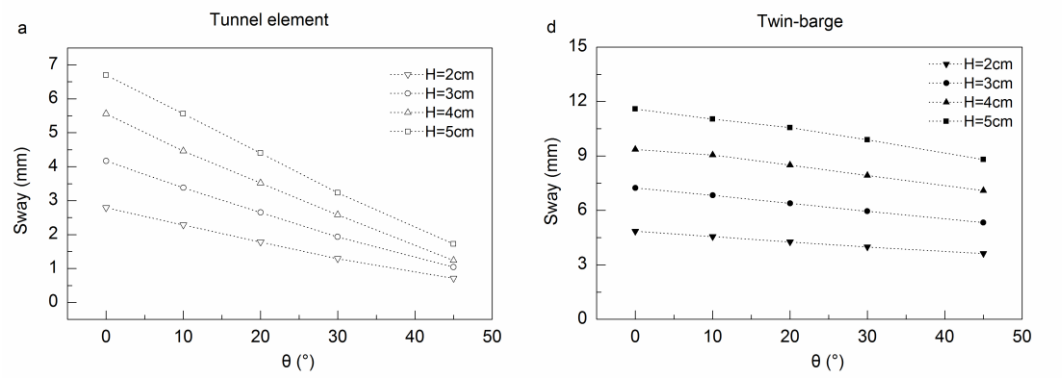

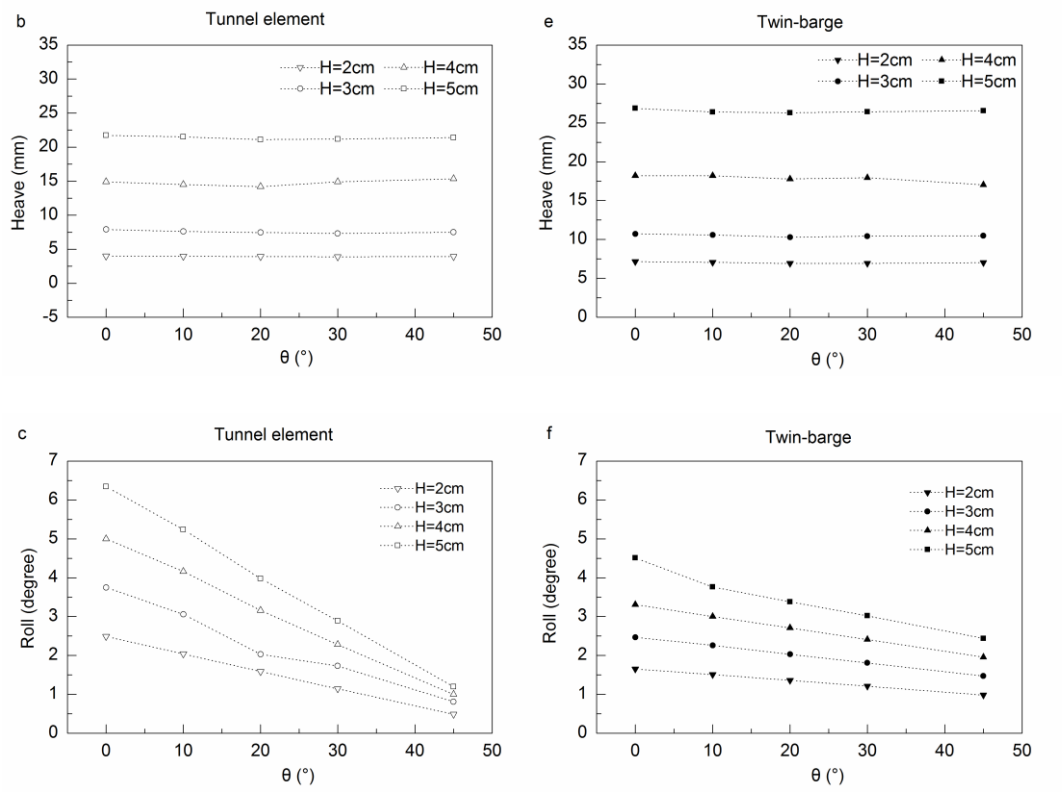

Fig. 20 The motion response of the tunnel element with mooring lines in different wave propagation directions T = 1.1sec, d = 0.2m. (hollow scatter: tunnel element, solid scatter: twin-barge)

Figs. 21a-c shows the relative difference derived from equation (3) between the twin-barge and the tunnel element, where the motion of the tunnel element is used as a reference. The relative difference for sway wave mode $\Delta\delta_{S\_wave}$, heave wave mode $\Delta\delta_{H\_wave}$ and roll wave mode $\Delta\delta_{R\_wave}$ are presented in Figs. 21a-c, respectively. It can be seen that the motion differences between the tunnel and twin-barge increase with the increasing wave incidence angle, and the relative values vary little with the incident wave height for sway and roll motions. However, a change in relative difference can be observed for the heave response that could potentially contributed to the change in wave particle velocity variations across the different wave heights tested, which vary between u = 0.0298m/s to 0.0746m/s for wave heights between H = 0.02m to 0.05m, respectively.

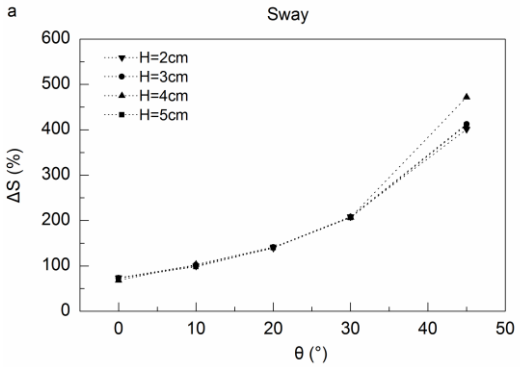

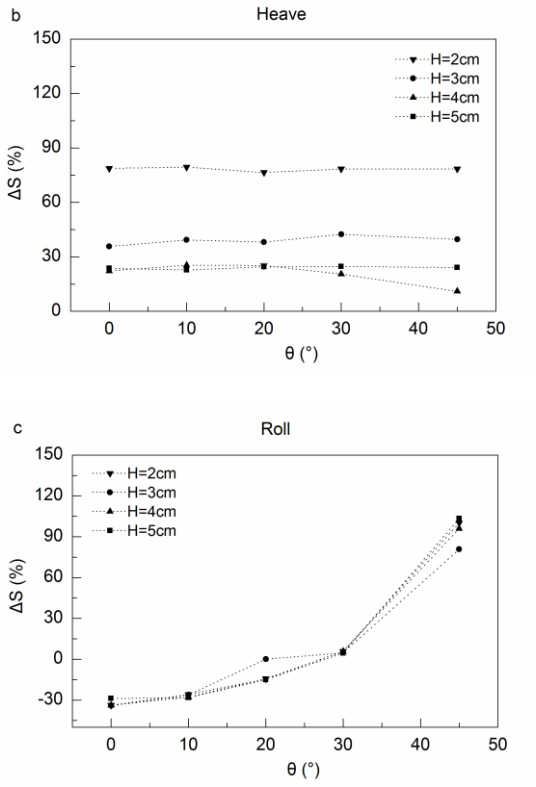

Fig. 21 Comparison of the motions between the tunnel element and twin-barge with different wave incidence angles

4 Conclusions and Future work

In this paper, experimental and numerical results for a moored tunnel element suspended by a twin-barge are presented for different regular wave conditions, tunnel element immersion depths, wave incident angles, and mooring configurations. The influence of the wave characteristics and the effect of the mooring lines and suspension cables on the tunnel element motions have been analyzed.

The study on the influence of these parameters on the motion of the tunnel element was initially implemented by obtaining the response of the tunnel element coupled to the twin-barge and fixed to a platform. The results demonstrated that the tunnel roll motion increases when coupled to the twin-barge. An analysis of the tunnel element with and without the tunnel element mooring lines was further investigated, where the tunnel element was coupled to the twin-barge. The study identified that the addition of the tunnel element mooring lines decreased the tunnel sway and roll motions, but increased the heave motion response. A general conclusion can be made that the addition of the tunnel element mooring lines has limited practical value, although this is likely to depend on the application being considered.

A detailed study of the impact of the tunnel element motion related to different immersion depths concluded that for sway, heave and roll modes the response of the tunnel element decreases for larger immersion depths. In sway two excitation modes were observed for the tunnel element, at the natural frequency of the tunnel element (low frequency mode) and the wave frequency mode, respectively. The response amplitude in the low frequency sway mode increases with immersion depth.

Comparing the tunnel element with the twin-barge for different wave incident angles and wave heights over a range of wave frequencies, it was observed that larger waves cause an increase in response for both tunnel element and twin-barge. A further observation was made that the percentage difference between the tunnel element and the

twin-barge is not significant for the different wave heights in the sway and roll modes, but increases for larger wave incident angles. In contrary in the heave wave frequency mode the percentage difference is similar over the range of wave incident angles but decreases with an increase in wave height.

Overall the study presents the response characteristics of the tunnel element in regular waves and has been used to calibrate and validate a numerical model. Future work will include the study of the response of the tunnel element during installation in irregular sea states which are representative of an installation location. Whilst this study identified that an additional tunnel element mooring line has limited effects to the stability of the tunnel element, it is suggested to consider different azimuth angles for the suspension cables to obtain clarity on enhanced stability of the tunnel element. The suggested future work would further include: 1) additional fully dynamic simulations to calibrate and validate the numerical model; 2) an extended range of wave conditions (i.e. wave height, period and direction) to investigate resonance behaviour; 3) include studies of the lowering operation and wave-current effects in the model.

Acknowledgement

The study is supported by the National Natural Science Foundation of China (Grant No.11272079) and the China Scholarship Council (award to Yang Can for 1 year's study abroad at the University of Exeter).

References

[1] Glerum A. Developments in immersed tunnelling in Holland[J]. Tunnelling and Underground Space Technology, 1995, 10(4): 455-462.

[2] Janssen W, Haas P D, Yoon Y H. Busan–Geoje Link: Immersed tunnel opening new horizons[J]. Tunnelling & Underground Space Technology; 2006, 21(3):332-332.

[3] Kasper, T., Steenfelt, J. S., Pedersen, L. M., Jackson P. G. & Heijmans, R. W. M. G. (2008). Stability of and Immersed Tunnel in Offshore Conditions under Deep Water Wave Impact. Coastal Engineering; 2008, August, 55(9): 753-760.

[4] Ingersley L. C. F. Considerations and strategies behind the design and construction requirements of the istanbul strait immersed tunnel[J]. Tunnelling and Underground Space Technology; 2005, 20(6):604-608.

[5] Ding, J.-H., Jin, X.-L., Guo Y.-Z. and Li., G.-G., "Numerical Simulation for Large-scale Seismic Response Analysis of Immersed Tunnel", Engineering Structures; 2006, 28(10):.1367-1377.

[6] Anastasopoulos I., Gerolymos N., Drosos V., Kourkoulis R., Georgarakos T. and Gazetas G., "Nonlinear Response of Deep Immersed Tunnel to Strong Seismic Shaking", Journal of Geotechnical and Geoenviron-mental Engineering; 2007, 133(9): 1067-1090.

[7] Jensen O P, Olsen T H, Kim C W, et al. Construction of immersed tunnel in off-shore wave conditions Busan-Geoje project South Korea [J]. Tunnelling and Underground Space Technology; 2006, 21:333.

[8] Aono T., Sumida K., Fujiwara R., Ukai A., Yamamura K. and Nakaya Y., 2003. Rapid stabilization of the immersed tunnel element. Proceedings of the Coastal Structures 2003 Conference, Portland Oregon.

[9] Chen Z, Zheng B, He J, et al. Experimental investigation on motions of immersing tunnel element under irregular wave actions[M]. INTECH Open Access Publisher; 2012.

[10] Zuo W., Wang Y.. Experimental investigation of motion responses of tunnel element immerging by moored barge [J]. Journal of Hydrodynamics, Ser. B 2015, 27(6):857-864.

[11] Harnois V, Weller S D, Johanning L, et al. Numerical model validation for mooring systems: Method and application for wave energy converters. Renewable Energy, 2015, 75: 869-887.

[12] Morison J R, O'Brien M D, Johnson J W, and Schaaf S A, 1950. The force exerted by surface waves on piles. Petrol Trans AIME. 189.

[13] Orcina. Orcaflex manual. 2013

[14] DNV. Offshore standard DNV-OS-E301, Position mooring. 2010.

[15] Bureau Veritas, 2002. NR 493 R02 E, Classification of Mooring Systems for Permanent Offshore Units.

[16] Khan, N.U., Ansari, K.A., 1986. On the dynamics of a multicomponent mooring line. Comput. Struct. 22, 311–334.

[17] Walton, T.S., Polachek, H., 1959. Calculation of Nonlinear Transient Motion of Cables. Technical Report. David Taylor Model Basin. Washington, D.C., USA.

[18] Yang C, Wang Y X, Zuo W G. Numerical simulations on the motion of immerged tunnel element with different arrangement types of mooring lines. The Ocean Engineering; 2014,32 (1),32-40. (in Chinese)

[19] Chen Z.J., Wang Y.X., Wang G.Y. and Hou Y., 2009. Experimental investigation on immersion of tunnel element. 28th International Conference on Ocean, Offshore and Arctic Engineering, Honolulu, Hawaii, America, OMAE2009-79073.